X-ray Photoelectron Spectroscopy Study of Rare-Earth Filled Skutterudites $LaFe_4P_{12}$ and $CeFe_4P_{12}$

Andrew P. Grosvenor,* Ronald G. Cavell, and Arthur Mar

Department of Chemistry, University of Alberta, Edmonton, Alberta, Canada T6G 2G2

Received November 28, 2005

The electronic structure of the rare-earth filled skutterudites $LaFe_4P_{12}$ and $CeFe_4P_{12}$ was examined by high-resolution core-line and valence-band X-ray photoelectron spectroscopy (XPS). From analysis of the binding energies and line shapes in the core-line spectra, the formulations $(La^{3+})(Fe^{2+})_4(P^-)_{12}$ and $(Ce^{3+})(Fe^{2+})_4(P^-)_{12}$ were obtained, with the electron deficiency being represented by a hole in the valence band. The occurrence of trivalent cerium was confirmed by the presence of a partially filled 4f state found in the valence band spectrum of $CeFe_4P_{12}$ but not in $LaFe_4P_{12}$. The valence band spectra agree well with the density of states determined from band structure calculations. These spectra were fitted through a simple model in which component peaks are related to electron populations. Such an analysis gives atomic charges that are consistent with the formulations derived from the core-line spectra.

1. Introduction

Since their initial discovery by Jeitschko and Braun,[1] the ternary rare-earth transition-metal pnictides REM_4Pn_{12} (RE = La, Ce, Pr, Nd, Sm, Eu, Gd, Tb, Yb; M = Fe, Ru, Os; Pn = P, As, Sb),[2] especially the antimonide members, have received considerable attention because of their potential as thermoelectric materials at high temperatures.[3] Their cubic structure is based on that of the parent mineral $CoAs_3$, called skutterudite,[4] which is adopted by other binary transition-metal pnictides MPn_3 (M = Co, Rh, Ir; Pn = P, As, Sb).[5,6] The crystal structure consists of a network of corner-sharing transition-metal-centered octahedra, which undergo a tilting distortion to form nearly square Pn_4 rings and large voids that are filled by RE atoms in the ternary variants (Figure 1). In some of the rare-earth filled antimonide skutterudites, such as $LaFe_4Sb_{12}$, the displacement parameters of the RE atoms within these irregular dodecahedral cages of pnicogen atoms are unusually large.[7] It has become fashionable to attribute the improved thermoelectric properties of these antimonides to a propitious combination of poor thermal conductivity (created by the "rattling" of the RE atoms, which scatters lattice vibrations) and good electrical conductivity, a model known as a "phonon-glass electron-crystal".[8] A detailed understanding of the electronic structure of these skutterudites is thus important for further development of these materials.

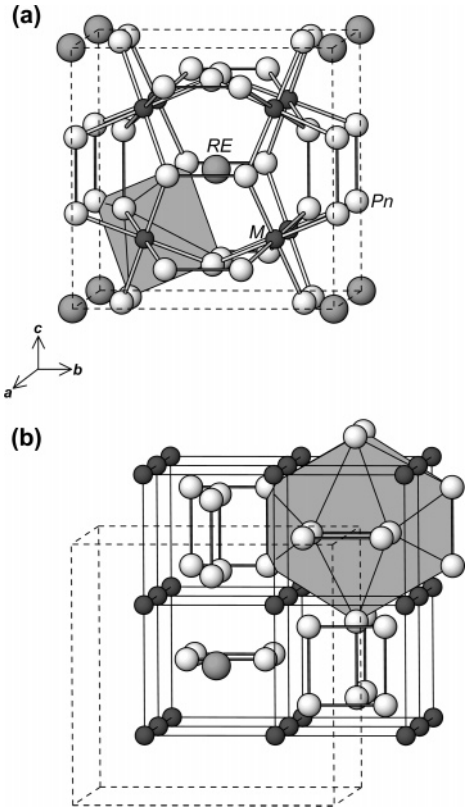

Figure 1. Filled skutterudite-type structure of ternary rare-earth transition-metal pnictides REM_4Pn_{12}, with the body-centered cubic unit cell outlined in dashed lines. The large gray spheres are RE atoms, the small solid spheres are M atoms, and the medium lightly shaded spheres are Pn atoms. (a) The framework of M-centered octahedra is emphasized. (b) An alternative representation highlights the cubic arrangement of M atoms enclosing the RE atoms (centered in a dodecahedral cage) and Pn_4 rings.

Although many experimental and theoretical studies have now been conducted on both the binary and ternary skutterudites, certain features of their electronic structure are still

* To whom correspondence should be addressed. E-mail: andrew.grosvenor@ualberta.ca.

(1) Jeitschko, W.; Braun, D. *Acta Crystallogr., Sect. B* **1977**, *33*, 3401−3406.
(2) Sales, B. C. In *Handbook on the Physics and Chemistry of Rare Earths*; Gschneidner, K. A., Jr., Bünzli, J.-C. G., Pecharsky, V. K., Eds.; Elsevier: Amsterdam, 2003; Vol. 33, pp 1−34.
(3) Nolas, G. S.; Morelli, D. T.; Tritt, T. M. *Annu. Rev. Mater. Sci.* **1999**, *29*, 89−116.
(4) Oftedal, I. *Zeitschrift fur Kristallographie* **1928**, *66*, 517−546.
(5) Rundqvist, S.; Errson, N.-O. *Ark. Kemi* **1968**, *30*, 103−114.
(6) Kjekshus, A.; Rakke, T. *Acta Chem. Scand.* **1974**, *A28*, 99−103.
(7) Braun, D. J.; Jeitschko, W. *J. Less-Common Met.* **1980**, *72*, 147−156.
(8) Slack, G. A. In *CRC Handbook of Thermoelectrics*; Rowe, D. M., Ed.; CRC Press: Boca Raton, FL, 1995; pp 407−440.

10.1021/cm052623n CCC: $33.50
Published on Web 02/18/2006

controversial. Some assertions derived from theoretical calculations[9−15] remain unconfirmed by experiment. In particular, there is conflicting evidence with regards to the valence state of specific atoms in these compounds. Although charge transfer is expected to be small in any of the rare-earth filled skutterudites, it will be most pronounced in the phosphides where electronegativity differences are the greatest and ambiguities in valence states are thereby more readily resolved.

In binary skutterudites such as CoP_3, an electron-counting scheme is easily derived by applying the Zintl concept, in which the more electropositive Co atoms are assumed to transfer a sufficient number of valence electrons so that the P atoms attain closed-shell configurations. An assignment of low-spin Co^{3+} (t_{2g}^6 e_g^0) accounts for the octahedral metal coordination and the observed diamagnetism,[16] and an assignment of P^- is consistent with the presence of P_4 rings with each P atom engaged in two $2c-2e^-$ P−P bonds. Extrapolated to a band picture in which the metal 3d, 4s, and 4p orbitals and the phosphorus 3s and 3p orbitals interact with each other within the extended structure, the electronic structure of the solid consists of filled M−P bonding and metal-based t_{2g} levels at lower energy and empty metal-based e_g and M−P antibonding levels at higher energy.[9] Overlaid on this energy-level diagram are filled P−P bonding and empty P−P antibonding levels. Although an energy gap is expected between the filled t_{2g} and empty e_g bands, more subtle effects conspire to close this gap so that most binary skutterudites are narrow or zero band gap semiconductors, as has been predicted by calculations and confirmed by experiments.[10,12−15]

In ternary skutterudites such as $LaFe_4P_{12}$, the rare-earth atoms can be considered to donate their valence electrons to the rest of the framework, $La^{3+}[Fe_4P_{12}]^{3-}$. If P^- is assumed in analogy with the binary skutterudites, then the average valence state of $Fe^{2.25+}$ implies that $LaFe_4P_{12}$ contains a partly filled t_{2g} band, with perhaps a single hole localized on one of the Fe atoms (i.e., three Fe^{2+} (t_{2g}^6 e_g^0) and one Fe^{3+} (t_{2g}^5 e_g^0) per $[Fe_4P_{12}]^{3-}$ unit).[2,9] Resistivity measurements confirm that $LaFe_4P_{12}$ is a hole-doped metal that becomes superconducting below 4.1 K.[17,18] However, magnetic measurements and Mössbauer spectra show that only low-spin Fe^{2+} is present.[19−21] Band structure calculations suggest that the valence states may be closer to Fe^{2+} and $P^{11/12-}$, implying that the hole is associated with 1 out of 12 P atoms.[9] The hole may reside in P−P nonbonding orbitals located close to the Fermi level (E_f).

$CeFe_4P_{12}$ was originally thought to contain tetravalent cerium (Ce^{4+}, $4f^0$), given the pronounced deviation of its cell parameter from the expected trend arising from the lanthanide contraction compared to other $REFe_4P_{12}$ members.[1] According to the assignment $Ce^{4+}[Fe_4P_{12}]^{4-}$, the $[Fe_4P_{12}]^{4-}$ (or $[FeP_3]^-$) framework is isoelectronic with CoP_3 and should thus lead to similar properties. Although electrical measurements confirm that $CeFe_4P_{12}$ is a small band gap semiconductor and magnetic measurements reveal a low magnetic susceptibility,[22] density functional calculations argue for a trivalent state for cerium (Ce^{3+}, $4f^1$) and indicate that the energy gap really arises because of the important contribution of rare-earth 4f orbitals to bonding states near the Fermi level.[11] X-ray absorption near-edge spectroscopy supports the assignment of trivalent Ce.[23,24]

We report here an experimental analysis of the electronic structure of the ternary phosphides $LaFe_4P_{12}$ and $CeFe_4P_{12}$ using high-resolution X-ray photoelectron spectroscopy (XPS) to access the valence states of all atoms during the same experiment. The RE, Fe, and P core-line spectra have been measured and have been interpreted in relation to the spectra of model compounds. The fitted valence band spectra of $LaFe_4P_{12}$ and $CeFe_4P_{12}$ are presented and compared to calculated band structures, which has permitted a detailed discussion of the bonding in these compounds, including the identification of Ce $4f^1$ states near the Fermi level.

2. Experimental Section

2.1. Synthesis. In accordance with previously reported methodology,[19] samples of $LaFe_4P_{12}$ and $CeFe_4P_{12}$ were prepared by direct reaction of the elements with excess red P and use of a Sn flux in sealed and evacuated fused-silica tubes (La, 99.9%, Alfa-Aesar; Ce, 99.9%, Cerac; Fe, 99.9%, Cerac; P, 99.995%, Cerac; Sn, 99.8%, Cerac). The RE:Fe:P:Sn molar ratio was 1:4:20:50. The tubes were heated to 950 °C over 30 h, cooled to 800 °C over 10 h, and held at this temperature for 1 week before being cooled to room temperature over 2 days. Once the reactions were complete, the product was carefully treated with dilute HCl (1:1) to remove the Sn flux as well as excess P and any binary phosphides or oxides that had formed. (*Caution*: some excess P may be transformed to the white allotrope, which is pyrophoric.) This treatment did not appear to decompose the ternary phosphides, which are dark gray, polycrystalline (individual crystals were 0.05−0.10 mm in size), and air-stable. Powder X-ray diffraction (XRD) patterns, obtained on an Inel diffractometer equipped with a CPS 120 detector, confirmed that the samples consisted of the desired ternary phosphides, with trace amounts of elemental phosphorus.

2.2. XPS Analysis. All measurements were performed on a Kratos AXIS 165 spectrometer with a monochromatic Al Kα X-ray

(9) Jung, D.; Whangbo, M.-H.; Alvarez, S. *Inorg. Chem.* **1990**, *29*, 2252−2255.
(10) Singh, D. J.; Pickett, W. E. *Phys. Rev. B* **1994**, *50*, 11235−11238.
(11) Nordström, L.; Singh, D. J. *Phys. Rev. B* **1996**, *53*, 1103−1108.
(12) Llunell, M.; Alemany, P.; Alvarez, S.; Zhukov, V. P.; Vernes, A. *Phys. Rev. B* **1996**, *53*, 10605−10609.
(13) Fornari, M.; Singh, D. J. *Phys. Rev. B* **1999**, *59*, 9722−9724.
(14) Lefebvre-Devos, I.; Lassalle, M.; Wallart, X.; Olivier-Fourcade, T.; Monconduit, L.; Jumas, J. C. *Phys. Rev. B* **2001**, *63*, 125110-1−125110-7.
(15) Kurmaev, E. Z.; Moewes, A.; Shein, I. R.; Finkelstein, L. D.; Ivanovskii, A. L.; Anno, H. *J. Phys.: Condens. Matter* **2004**, *16*, 979−987.
(16) Ackermann, J.; Wold, A. *J. Phys. Chem. Solids* **1977**, *38*, 1013−1016.
(17) Meisner, G. P. *Physica B* **1981**, *108*, 763−764.
(18) Torikachvili, M. S.; Chen, J. W.; Dalichaouch, Y.; Guertin, R. P.; McElfresh, M. W.; Rossel, C.; Maple, M. B.; Meisner, G. P. *Phys. Rev. B* **1987**, *36*, 8660−8664.
(19) Grandjean, F.; Gérard, A.; Braun, D. J.; Jeitschko, W. *J. Phys. Chem. Solids* **1984**, *45*, 877−886.
(20) Shenoy, G. K.; Noakes, D. R.; Meisner, G. P. *J. Appl. Phys.* **1982**, *53*, 2628−2630.
(21) Long, G. J.; Hautot, D.; Grandjean, F.; Morelli, D. T.; Meisner, G. P. *Phys. Rev. B* **1999**, *60*, 7410−7418.
(22) Meisner, G. P.; Torikachvili, M. S.; Yang, K. N.; Maple, M. B.; Guertin, R. P. *J. Appl. Phys.* **1985**, *57*, 3073−3075.
(23) Xue, J. S.; Antonio, M. R.; White, W. T.; Soderholm, L. *J. Alloys Compd.* **1994**, *207/208*, 161−164.
(24) Grandjean, F.; Long, G. J.; Cortes, R.; Morelli, D. T.; Meisner, G. P. *Phys. Rev. B* **2000**, *62*, 12569−12572.

source operating with a base pressure in the analytical chamber of 10^{-6} to 10^{-7} Pa. The resolution function of this instrument has been determined to be 0.4 eV on the basis of analysis of the Co Fermi edge.

Samples of $LaFe_4P_{12}$ and $CeFe_4P_{12}$ were ground and pressed onto C tape before being loaded into the instrument. Both samples were sputter-cleaned for nearly 1 h with an Ar^+ ion beam (4 kV, 10 mA) to remove surface contaminants (Sn, C, O, etc.). High-resolution spectra (La, Ce 3d; Fe 2p; P 2p; valence band) were then collected with energy envelopes ranging from 60 to 20 eV, a step size of 0.05 eV, a pass energy of 20 eV, a sweep time of 180 s, and an analysis spot size of 700 × 400 μm. Because these compounds are electrically conducting, charge neutralization was not required during the spectroscopic measurements and charge correction was not applied in the data analysis. All results were analyzed with use of the CasaXPS software package.[25] To fit these high-resolution spectra, a Shirley type function was used to remove the background, which arises largely from inelastic electron scattering. The extracted spectra were then fitted with a combined Gaussian (70%) and Lorentzian (30%) line profile to account for spectrometer and lifetime broadening, respectively.

To clarify the cerium valence state in $CeFe_4P_{12}$, several model compounds were also examined. The RE 3d and valence band spectra of CeF_3 (99.9%, Alfa-Aesar), CeF_4 (99.9%, Aldrich), LaP (prepared by direct reaction of the elements at 700 °C for 2 days, and sample purity confirmed by XRD), and LaF_3 (99.99%, Aldrich) were collected with parameters similar to those above. Because these compounds are insulating, they were pressed into In foil to increase conductivity and were transported to the spectrometer under Ar to reduce reaction with the environment. The charge neutralizer was used (current = 1.7 A, charge balance = 1.8 V) during collection, and the spectra were charge-corrected during data analysis by setting the adventitious C 1s binding energy to 284.8 eV.

2.3. Band Structure Calculations. Although several theoretical calculations have been previously performed on skutterudite-type compounds,[9−15] it was desirable to extract partial density of states profiles for the metal and phosphorus valence states to illustrate our fitting of the experimental valence band spectra. We reproduce a tight-binding extended Hückel band structure calculation on the $[Fe_4P_{12}]^{3-}$ substructure of $LaFe_4P_{12}$,[9] with the same parameters and 125 *k* points in the irreducible portion of the Brillouin zone, but showing the projections of the Fe and P orbital contributions over a wider energy window to draw an explicit comparison to the experimental valence band spectrum.

3. Results and Discussion

3.1. High-Resolution P 2p Spectra. Figure 2 shows the P 2p spectra of $LaFe_4P_{12}$ and $CeFe_4P_{12}$. Both spectra reveal P $2p_{3/2}$ binding energies (BE) of 129.3 eV, which is identical to that found in FeP, where a charge of −1.0 on the phosphorus atom was established through comparison with other Fe- and P-containing compounds with well-defined oxidation states.[26] Homoatomic phosphorus-bonded units are present in the form of P_4 rings in $REFe_4P_{12}$ and zigzag chains in FeP, but whereas the P−P distances in $LaFe_4P_{12}$ (2.288(2)−2.356(2) Å)[1] are similar to a typical single P−P covalent bond length of 2.2 Å,[27] they are somewhat longer

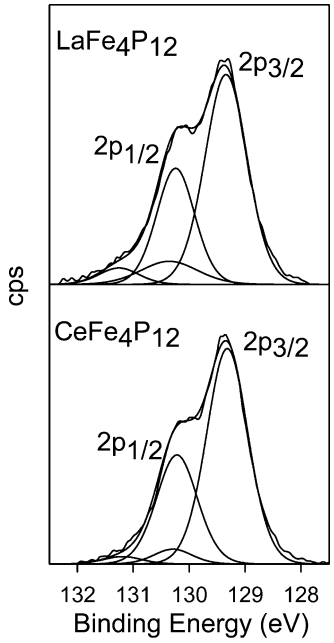

Figure 2. High-resolution P 2p XPS spectra of $LaFe_4P_{12}$ and $CeFe_4P_{12}$.

in FeP (2.643(4) Å).[28] Nevertheless, it appears that, in both cases, the prediction of a formal P^- charge on the phosphorus atoms bound to two P neighbors, from a simple electron-counting scheme in which 2c−2e$^-$ P−P bonds are assumed, is in good agreement with the charges extracted from the binding energies. Instead of P^-, an alternative assignment of $P^{11/12-}$ has also been predicted,[9] but of course these charges are so similar that they cannot be distinguished by examining binding energies. Moreover, because the bonding is probably delocalized within the P_4 rings, it is perhaps more accurate to represent the charges as P_4^{4-}. As anticipated from the XRD pattern, the spectrum also shows the presence of unreacted elemental phosphorus, with a $2p_{3/2}$ binding energy of 130.3 eV.

These results can be compared with those obtained from XPS studies of the binary skutterudite $CoSb_3$.[29] The difference between the P $2p_{3/2}$ binding energy in $REFe_4P_{12}$ and that in elemental P is substantially greater (ΔBE = 1.0 eV) than that between the Sb $3d_{5/2,3/2}$ binding energy in $CoSb_3$ and that in elemental Sb (ΔBE = 0.2 eV). This observation can be attributed to the diminished electronegativity differences on going from the phosphide to the antimonide and is consistent with the trend toward less ionic character in the Co−Sb bond than in the Fe−P bond.

3.2. High-Resolution Fe 2p Spectra. The Fe 2p spectra of $LaFe_4P_{12}$ and $CeFe_4P_{12}$ are presented in Figure 3. In both spectra the Fe $2p_{3/2}$ signal appears as a single core line with asymmetric line shapes skewed to higher binding energy. As indicated earlier, assignments of $Fe^{2.25+}$ or Fe^{2+} have been proposed from electron-counting schemes.[2,9] The assignment of $Fe^{2.25+}$ corresponds to mixed valency, with Fe^{2+} and Fe^{3+} present in the ratio 3:1, which would be manifested as two distinct Fe 2p signals with intensities in the same ratio.

(25) Fairley, N. *CasaXPS*, version 2.2.19; Casa Software, Ltd.: Teighnmouth, Devon, U.K., 2003 (www.casaxps.com).
(26) Grosvenor, A. P.; Wik, S. D.; Cavell, R. G.; Mar, A. *Inorg. Chem.* **2005**, *24*, 8988−8998.
(27) Pauling, L. *The Nature of the Chemical Bond*, 3rd ed.; Cornell University Press: Ithaca, NY, 1960.
(28) Rundqvist, S.; Nawapong, P. C. *Acta Chem. Scand.* **1965**, *19*, 1006−1008.
(29) Anno, H.; Matsubara, K.; Caillat, T.; Fleurial, J.-P. *Phys. Rev. B* **2000**, *62*, 10737−10743.

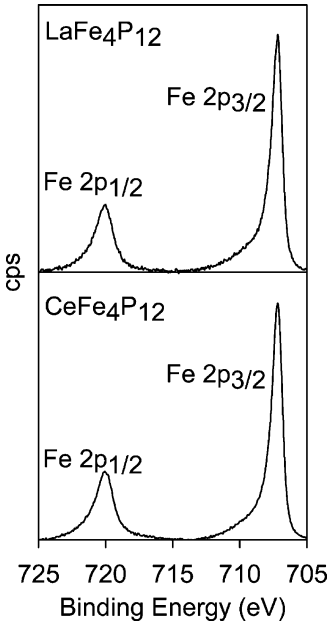

Figure 3. High-resolution Fe 2p XPS spectra of $LaFe_4P_{12}$ and $CeFe_4P_{12}$.

During a previous XPS study of the reduction of $K_3Fe(CN)_6$, the $2p_{3/2}$ binding energy of low-spin Fe^{3+} was observed to be noticeably higher than that of low-spin Fe^{2+}.[30] When the compound was heavily reduced, so that only a small amount of Fe^{3+} remained, the $2p_{3/2}$ spectrum appeared to broaden with an apparent asymmetric tail to higher binding energy, similar to the $2p_{3/2}$ feature observed in Figure 3. However, the $2p_{1/2}$ spectrum of the reduced ferricyanide clearly showed a doublet, which arises from the presence of two distinct Fe valence states.[30] In contrast, as seen in Figure 3, the $2p_{1/2}$ signals for $LaFe_4P_{12}$ and $CeFe_4P_{12}$ are asymmetric and appear similar to the $2p_{3/2}$ signals, leading to the conclusion that only one Fe valence state is present in these compounds. Moreover, the Fe $2p_{3/2}$ binding energy (707.2 eV) is similar to that in FeS_2 (707.0 eV), which is well-known to contain low-spin Fe^{2+}.[31] It should also be noted that the spectra of low-spin Fe^{2+} compounds such as those shown here do not suffer the effects of multiplet splitting, which tends to broaden the 2p spectra of high-spin Fe^{2+} compounds.[32] The definitive finding of low-spin Fe^{2+} ($t_{2g}^6\ e_g^0$) in $LaFe_4P_{12}$ and $CeFe_4P_{12}$ supports results obtained by Mössbauer spectroscopy.[19−21]

What, then, is the origin of the asymmetric tail? Doniach and Šunjić have proposed that this type of line shape arises when valence electrons, interacting with the core hole (produced after photoionization), are excited and scattered from filled states below the Fermi edge to empty conduction states above.[33] If there is a continuum of states above and below the Fermi edge, then an asymmetric tail comprising many closely spaced states is observed instead of a few distinct satellite peaks.[34] This process is typically indicative

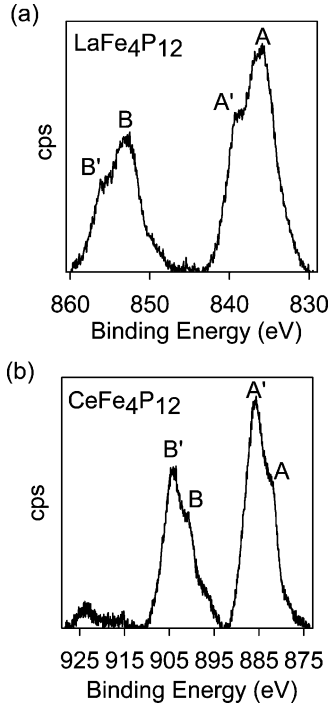

Figure 4. (a) High-resolution La 3d XPS spectrum of $LaFe_4P_{12}$ and (b) Ce 3d XPS spectrum of $CeFe_4P_{12}$. The $3d_{5/2}$ core line is labeled A, and the $3d_{3/2}$ core line is labeled B. The most intense satellite peaks are labeled A′ and B′.

of metal−metal bonding, but the Fe−Fe distances exceed 3.9 Å in these compounds. Calculations suggest that electronic conduction proceeds through bands near the Fermi level that arise from interactions between nonbonding or bonding orbitals on the P_4 rings and s,p orbitals on the transition-metal atoms.[9,12] The asymmetric line shape may then perhaps reflect some delocalization of the metal electrons, which may account for the weak paramagnetism observed in these compounds.[19,35]

3.3. High-Resolution RE 3d Spectra. Figure 4 shows the RE 3d spectra for $LaFe_4P_{12}$ and $CeFe_4P_{12}$. Normally, as in most transition metals, the binding energy in the elemental metal is generally lower than in the oxidized species. Surprisingly, this is not the case in the RE spectra. For example, the $3d_{5/2}$ binding energy is 884 eV in Ce metal,[36,37] whereas it is 882 eV in $CeCl_3$ and CeO_2.[38,39] This unusual behavior may be traced to the poor screening of the nuclear charge offered by 4f electrons. Although the binding energy in RE spectra is not necessarily diagnostic of the valence state, the line shape is quite characteristic of the valence state, especially for Ce compounds. The spectra of these rare-earth skutterudites can then be interpreted by making comparisons to those of model compounds.

For $LaFe_4P_{12}$, the binding energy of the La $3d_{5/2}$ core line (labeled *A* in Figure 4a) is 836.1 eV, which is similar to that

(30) Wallbank, B.; Johnson, C. E.; Main, I. G. *J. Electron Spectrosc. Relat. Phenom.* **1974**, *4*, 263−269.
(31) Nesbitt, H. W.; Muir, I. J. *Geochim. Cosmochim. Acta* **1994**, *58*, 4667−4679.
(32) Grosvenor, A. P.; Kobe, B. A.; Biesinger, M. C.; McIntyre, N. S. *Surf. Interface Anal.* **2004**, *36*, 1564−1574.
(33) Doniach, S.; Šunjić, M. *J. Phys. C: Solid State Phys.* **1970**, *3*, 285−291.
(34) Hüfner, S. In *Photoemission in Solids II*; Ley, L., Cardona, M., Eds.; Springer-Verlag: Berlin, 1979.
(35) Danebrock, M. E.; Evers, C. B. H.; Jeitschko, W. *J. Phys. Chem. Solids* **1996**, *57*, 381−387.
(36) Schlapbach, L.; Osterwalder, J.; Siegmann, H. C. *J. Less-Common Met.* **1982**, *88*, 291−297.
(37) Schlapbach, L.; Osterwalder, J. *Solid State Commun.* **1982**, *42*, 271−274.
(38) Park, K.-H.; Oh, S.-J. *Phys. Rev. B.* **1993**, *48*, 14833−14842.
(39) Dauscher, A.; Hilaire, L.; Le Normand, F.; Mueller, W.; Maire, G.; Vasquez, A. *Surf. Interface Anal.* **1990**, *16*, 341−346.

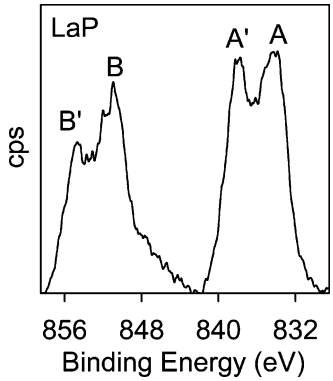

Figure 5. High-resolution La 3d XPS spectrum of LaP. The $3d_{5/2}$ and $3d_{3/2}$ core lines are labeled A and B, respectively. The most intense satellite peaks are labeled A′ and B′.

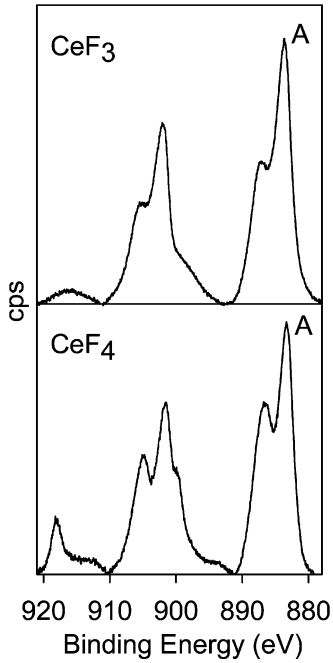

Figure 6. High-resolution Ce 3d XP spectra of CeF_3 and CeF_4, showing the difference between the Ce^{3+} and Ce^{4+} line shapes. The $3d_{5/2}$ core line is labeled A in each spectrum.

in $LaCl_3$ (836 eV)[38] but higher than in LaP (834.3 eV; Figure 5). The $3d_{5/2}$ line shapes for all three compounds resemble each other, which leads to the unsurprising conclusion of a La^{3+} valence state. However, in addition to the core lines (labeled A and B for the $3d_{3/2}$ and $3d_{5/2}$ peaks, respectively), there are strong satellite peaks (labeled A′ and B′), whose origins will be discussed below.

For $CeFe_4P_{12}$, assignments of Ce^{3+} or Ce^{4+} have been proposed.[1,2,23,24] CeF_3 and CeF_4 serve as appropriate comparisons, and their spectra are shown in Figure 6. As anticipated, the line shapes differ markedly for Ce^{3+} and Ce^{4+}. There are more peaks in the Ce^{4+} spectrum because of the possibility for different final state 4f fillings ($4f^{0,1,2}$).[40] The spectrum of $CeFe_4P_{12}$ agrees well with that of CeF_3 and has a $3d_{5/2}$ core-line binding energy (labeled A in Figure 4b) of 882.0 eV. This comparison confirms the presence of trivalent Ce in $CeFe_4P_{12}$.

In the 3d spectra of all of these rare-earth compounds, distinct satellite peaks appear at 3.5−4.0 eV above the $3d_{5/2}$ and $3d_{3/2}$ core lines. Several theories have been developed to explain the formation of such satellites. One theory, called the shake-up model, invokes a transition whereby a valence electron located on a metal center is promoted to an empty state above the Fermi level following the photoionization event.[41] The cross section of this satellite peak has been suggested to be influenced by the degree of overlap between the metal and the ligand.[42] Increased orbital overlap between the ligand and the metal allows for an increased presence of electrons near the metal able to screen the core hole on the metal produced during the photoionization process. This increased screening allows for an increase in the cross section of the promotion of an electron from a filled valence state on the metal to an empty conduction state. With highly electronegative ligands such as F, orbital overlap is poorer than with less electronegative ligands such as P, and the satellite intensity should diminish. For example, the intensity of the satellite peaks found in the $3d_{5/2}$ spectra of lanthanum trihalides, LaX_3, decreases as the ligand is changed from I to F.[43] In the compounds containing La^{3+}, the satellite peak is found only ∼3.5 eV above the core line. Although empty La 4f states located about 4−6 eV beyond the Fermi level exist,[38] there are no filled La states within the valence band, so intraatomic shake-up can be ruled out as the cause of this satellite peak. In the compounds containing Ce^{3+}, there is a partially filled 4f state within the valence band ($4f^1$), so intraatomic shake-up cannot be ruled out as a cause of the satellite.

A more reasonable model that can account for the presence of satellite peaks in the spectra of both the La^{3+} and the Ce^{3+} compounds is ligand-to-metal charge-transfer shake-up.[38,42] This transition involves the promotion of a valence electron on a ligand to an empty state on the metal center above the Fermi level, after the metal is photoionized and a core hole is produced.[42] These conditions are satisfied for both the La and the Ce 3d spectra, where empty RE 4f states reside about 4−6 eV above the Fermi level and filled ligand states are present near the Fermi level.[9,11,13] The cross section for this process is again controlled by the degree of orbital overlap between the metal and ligand as well as the ability of the ligand valence electrons to relax toward the empty conduction states on the metal after production of the core hole.[42] Less electronegative ligands allow for easier relaxation of the valence electrons toward the metal center, and, therefore, the cross section of the satellite is larger if less electronegative ligands are available rather than those having a larger electronegativity.[42] The satellite intensities and core-line binding energies for $LaFe_4P_{12}$ (Figure 4a) and LaP (Figure 5) are not identical even though P atoms surround the La centers in both cases, because the coordination numbers and environments are different. The satellite peak is more intense in $CeFe_4P_{12}$ than in $LaFe_4P_{12}$ (Figure 3), which is consistent with the establishment of a greater orbital

(40) Kaindl, G.; Wertheim, G. K.; Schmiester, G.; Sampathkumaran, E. V. *Phys. Rev. Lett.* **1987**, *58*, 606−609.
(41) Imada, S.; Jo, T. *J. Phys. Soc. Jpn.* **1989**, *58*, 402−405.
(42) Sarma, D. D.; Vishnu Kamath, P.; Rao, C. N. R. *Chem. Phys.* **1983**, *73*, 71−82.
(43) Uwamino, Y.; Tsuge, A.; Ishizuka, T.; Yamatera, H. *Bull. Chem. Soc. Jpn.* **1986**, *59*, 2263−2267.

overlap arising from the presence of a $4f^1$ state within the valence band.

Because P and Fe atoms surround the RE atoms, it might be expected that, reciprocally, similar satellite peaks may be found in their spectra. Previous work has shown that if the ligand bonds to the metal through p orbitals, then the ligand electronic states will be less affected by the ligand-to-metal charge-transfer process and no satellite peak will appear.[42] Because the P atoms interact with the RE atoms largely through 3p orbitals, no satellite peak should appear in the P spectrum, as confirmed in Figure 2. If the Fe atoms interact significantly with the RE atoms through 3d orbitals, then a satellite peak would be expected, but none was observed (Figure 3). Such a satellite peak is predicted to be located above the core line at a binding energy much higher than is found in the RE spectra.[42] This is difficult to confirm by examining the P and Fe spectra, because strong energy loss occurs from interatomic effects such as plasmon loss and inelastic electron scattering, at energies in the range where these satellite peaks might be expected. All things considered, the ligand-to-metal charge-transfer shake-up model best accounts for the presence of satellite peaks observed in the La and Ce 3d spectra.

3.4. Valence Band Spectra. Valuable information about the bonding involved in solids can be gained by examining the occupation of the electronic states which can be derived from the valence band spectra. The interpretation of these spectra is aided by comparison with the density of states determined from band structure calculations. Below we illustrate how the spectrum of $LaFe_4P_{12}$ is analyzed through a fitting methodology that we have successfully applied elsewhere to binary transition-metal phosphides,[26] and then we extend the protocol to $CeFe_4P_{12}$.

The valence band spectrum of $LaFe_4P_{12}$ (Figure 7a) consists of three distinct regions: (i) a small doublet band from 15 to 8 eV, (ii) a broad band from 8 eV to the Fermi edge, and (iii) a narrow intense band, superimposed on the second region, from 3 eV to the Fermi edge. This spectrum closely resembles that of the binary skutterudite $CoSb_3$.[29] Because the La atoms can be considered, to a first approximation, to merely donate their valence electrons to the rest of the structure, no La valence states are expected within the valence band. The total density of states curve (Figure 7b), determined from a tight-binding extended Hückel band structure calculation on the $[Fe_4P_{12}]^{3-}$ substructure, reproduces the general features seen in the valence band spectrum, bearing in mind that experimental effects such as lifetime broadening and photoionization cross sections will introduce important differences in the observed intensities. Bonding within the remaining $[Fe_4P_{12}]^{3-}$ substructure then arises from the sharing of electrons between Fe and P atoms. One way to proceed with fitting is to assign features of the valence band spectrum to the contributing atomic orbitals that give rise to these electronic states in the solid. The projections of the P 3s, P 3p, and Fe 3d contributions to the total density of states (Figure 7b) correspond closely to the three gross binding energy regions identified respectively in the valence band spectrum. The electronic states can also be interrogated for their type of bonding character. The crystal orbital overlap

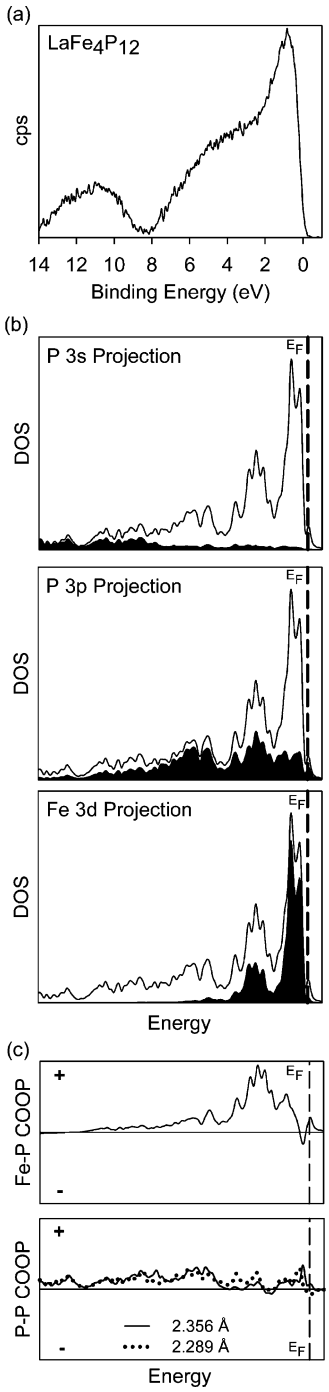

Figure 7. (a) Valence band spectrum of $LaFe_4P_{12}$. (b) Contributions of P 3s, P 3p, and Fe 3d orbitals (shaded regions) to the total density of states (line) for $LaFe_4P_{12}$. The dashed line marks the Fermi level. (c) COOP curves for Fe−P and P−P contacts in $LaFe_4P_{12}$.

population (COOP) curves (Figure 7c) indicate that Fe−P bonding states are constrained largely within an energy region close to the Fermi level, whereas P−P bonding states are spread out throughout the entire valence band.

On the basis of these assignments, the valence band spectrum for $LaFe_4P_{12}$ was fitted with a minimum number of peaks (Figure 8a). The binding energies and full width at half-maximum (fwhm) values of the component peaks are listed in Table 1. The doublet from 15 to 8 eV represents P 3s states and was fitted by two symmetric peaks having similar fwhm values. The broad band from 8 eV to the Fermi

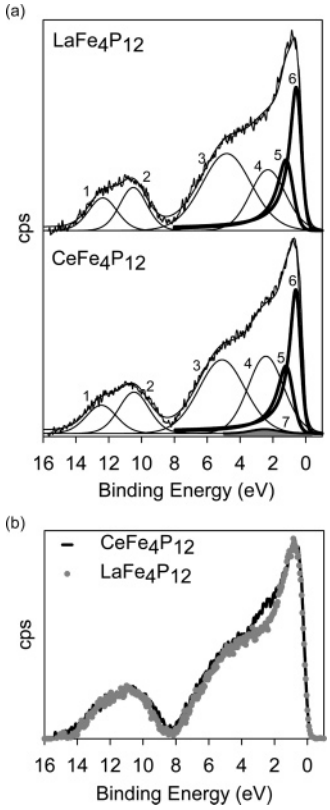

Figure 8. (a) Fitted valence band spectra of $LaFe_4P_{12}$ and $CeFe_4P_{12}$. The P peaks are represented by thin black lines, and the asymmetric Fe 3d peaks are represented by thick black lines. The Ce 4f state centered at 2.5 eV in the $CeFe_4P_{12}$ spectrum is represented by a filled gray peak. The identity of each peak is provided in Table 1. (b) Valence band spectra from $CeFe_4P_{12}$ and $LaFe_4P_{12}$ overlaid on each other. The difference between the two spectra is apparent at 2.5 eV and is attributed to the presence of a Ce 4f component in the $CeFe_4P_{12}$ spectrum.

Table 1. Binding Energies (eV) of Component Peaks in Valence Band Spectra of $LaFe_4P_{12}$ and $CeFe_4P_{12}$[a]

peak	assignment	$LaFe_4P_{12}$	$CeFe_4P_{12}$
1	P 3s A	12.4 (2.0)	12.4 (2.2)
2	P 3s B	10.5 (2.0)	10.5 (2.2)
3	P $3p_{3/2}$ A	4.8 (3.6)	5.1 (3.3)
4	P $3p_{3/2}$ B	2.3 (2.6)	2.4 (2.6)
5	Fe $3d_{3/2}$	1.2 (1.0)	1.2 (1.0)
6	Fe $3d_{5/2}$	0.6 (0.7)	0.6 (0.7)
7	Ce $4f_{7/2}$		2.5 (2.0)

[a] The fwhm values (eV) are indicated in parentheses.

edge was fitted by two P $3p_{3/2}$ states with a rather large fwhm. A better fit of this region can be achieved by invoking several pairs of $3p_{3/2}$ and $3p_{1/2}$ states in a fixed intensity ratio of 2:1 and an energy splitting similar to that observed in the P 2p core-line spectra (0.9 eV), but as the electron counts extracted from both analyses are similar, this extra parametrization was not deemed justifiable. The presence of more than one P 3s or P 3p component peak is unlikely to be attributable to multielectron excitation processes, as these are normally not pronounced in valence band spectra. A possible reason could be the distinction between the shorter (2.289 Å) and longer (2.356 Å) P−P bonds within the P_4 ring, which is not strictly square.[1] The inequivalence of these bonding states is manifested by a shift in energy in the P−P COOP curves in Figure 7c. A more enticing idea is that the two P $3p_{3/2}$ peaks represent states that are involved in the separate σ and π components of the P−P bonds within the P_4 ring.[9,12] Finally,

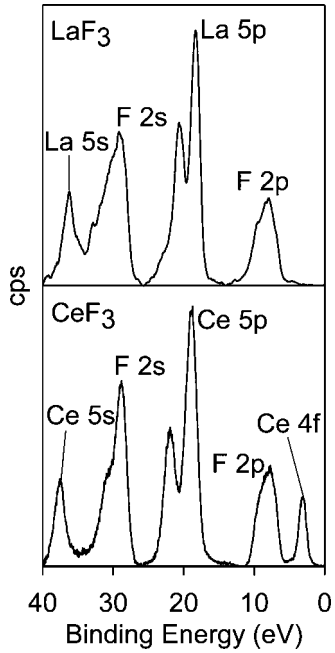

Figure 9. Valence band spectra of LaF_3 and CeF_3. The Ce 4f peak at ~3.1 eV is apparent in the CeF_3 spectrum with no similar component being observed in the LaF_3 spectrum.

the narrow band from 3 eV to the Fermi edge was fitted to two asymmetric peaks representing Fe $3d_{5/2}$ and $3d_{3/2}$ states with an intensity ratio of 3:2 and an energy splitting of 0.6 eV. The asymmetry of these peaks is similar to that found in the high-resolution Fe 2p core-line spectra (Figure 3).

The valence band spectrum of $CeFe_4P_{12}$ is also shown in Figure 8a and can be fit by component Fe and P peaks with energies and widths similar to those in $LaFe_4P_{12}$. However, an important difference is the appearance of an increased band intensity centered near 2.5 eV in the valence band spectrum of $CeFe_4P_{12}$ that is absent in that of $LaFe_4P_{12}$, as can be seen more clearly by overlaying the two spectra in Figure 8b. We interpret this feature as arising from a Ce $4f^1$ state located within the valence band, providing direct evidence for the presence of trivalent cerium. To support this interpretation, the valence band spectra of LaF_3 and CeF_3 were also recorded (Figure 9). A 4f signal was clearly observed in the spectrum of CeF_3 but not in LaF_3, at an energy (3.1 eV) similar to that for the 4f signal in $CeFe_4P_{12}$. Furthermore, the energy of the $4f^1$ state (2.8 eV) obtained during a recent resonant photoemission study of $CeFe_4P_{12}$ is close to that found here.[44] Thus, in the valence band spectrum of $CeFe_4P_{12}$, this additional component was assigned to a Ce $4f_{7/2}$ peak (shown as the filled gray region in Figure 8a) positioned at 2.5 eV with a fwhm of 2.0 eV. These results are consistent with predictions from density functional calculations, which show only empty 4f states in the conduction band for $LaFe_4P_{12}$ but filled 4f states in the valence band for $CeFe_4P_{12}$.[11,13] Moreover, in both cases, the sharpness of the Fermi edge in the valence band spectra is consistent with the location of the Fermi level lying just below the top of the valence band, as expected for these hole-doped materials.

(44) Ishii, H.; Miyahara, T.; Takayama, Y.; Obu, K.; Shinoda, M.; Lee, C.; Shiozawa, H.; Yuasa, S.; Matsuda, T. D.; Sugawara, H.; Sato, H. *Surf. Rev. Lett.* **2002**, *9*, 1257−1261.

Table 2. Corrections Applied to Peak Intensities in Valence Band Spectra of $LaFe_4P_{12}$ and $CeFe_4P_{12}$[a]

atom	state	photoionization cross section, σ	IMFP, λ (Å)
Ce	$4f_{7/2}$	0.078	25.1
Fe	$3d_{3/2}$	0.0694	25.9
	$3d_{5/2}$	0.1017	
P	$3s_{1/2}$	0.1116	33.9
	$3p_{3/2}$	0.0708	

[a] The P $3p_{3/2}$ cross sections were corrected on the basis of comparison of experimental cross sections determined by Brillson and Ceasar[46] to those calculated by Scofield.[47] All other cross sections listed are those calculated by Scofield.[47] These cross sections were determined for an excitation energy equal to that of Al Kα X-rays.[47] The IMFP values were determined using the QUASES IMFP calculator.[48]

Table 3. Electron Populations in $LaFe_4P_{12}$ and $CeFe_4P_{12}$

state	$LaFe_4P_{12}$	$CeFe_4P_{12}$
P 3s A	5.7	5.1
P 3s B	7.0	7.5
P 3p A	36.5	32.3
P 3p B	20.7	26.1
Fe 3d	25.1	23.6
Ce 4f		1.4
total number of e^-	95.0	96.0
calculated charge per atom	+3 (La),[a] +1.7 (Fe), −0.8 (P)	+2.6 (Ce), +2.1 (Fe), −0.9 (P)

[a] Assumed from analysis of the La 3d high-resolution spectrum.

In principle, the intensities of the component peaks in the fitted valence band spectra can be related to the electron populations of these states. However, the peak intensities (I) must be corrected for different photoionization cross sections (σ) and inelastic mean free paths (IMFP, λ) for each state. These values are listed in Table 2. The normalized peak intensities (C_i) can then be calculated from eq 1, which gives the fractional electron concentration for a given state.[45]

$$C_i = \frac{I_i/(\sigma_i\lambda_i)}{\sum_{j=1}^{n} I_j/(\sigma_j\lambda_j)} \quad (1)$$

In this equation, $I_i/(\sigma_i\lambda_i)$ represents the corrected intensity of the peak under consideration and $\sum_{j=1}^{n} I_j/(\sigma_j\lambda_j)$ represents the sum of the corrected intensities from all of the peaks present in the valence band spectrum. The number of electrons in each state can then be determined by multiplying C_i by the total number of valence electrons (95 for $LaFe_4P_{12}$ and 96 for $CeFe_4P_{12}$). The electron populations and atomic charges are listed in Table 3. For $LaFe_4P_{12}$, charges of +1.7 for Fe and −0.8 for P are found. (A charge of +3 is assumed for La because no 4f states are occupied.) For $CeFe_4P_{12}$, charges of +2.6 for Ce, +2.1 for Fe, and −0.9 for P are found. With the charges in good agreement with the results deduced from the core-line spectra, this type of population analysis serves as an independent check on the core results and demonstrates the usefulness of fitting valence band spectra.

4. Conclusion

The rare-earth filled skutterudites $LaFe_4P_{12}$ and $CeFe_4P_{12}$ have been examined by XPS for the first time. Analysis of the binding energies and line shapes in high-resolution core-line spectra for La, Ce, Fe, and P supports the formulations $(La^{3+})(Fe^{2+})_4(P^-)_{12}$ and $(Ce^{3+})(Fe^{2+})_4(P^-)_{12}$, where the electron deficiency is represented by a hole in the valence band. The binding energies of the P $2p_{3/2}$ core lines are characteristic of anionic phosphorus, although the negative charge is probably delocalized within the P_4^{4-} ring. The Fe 2p spectra indicate the presence of only low-spin Fe^{2+}, as indicated by the narrow core lines observed. The asymmetric line shapes in the Fe spectra suggest delocalization of the metal electrons via interaction with the P_4 rings. Characteristic line shapes of core lines in the RE 3d spectra indicate the presence of La^{3+} and Ce^{3+}. Intense satellite peaks in these spectra are attributed to ligand-to-metal charge-transfer shake-up processes. The enhanced intensity of the satellite peak in the Ce 3d spectrum is consistent with greater orbital overlap that would be imparted by the presence of a 4f state located within the valence band of $CeFe_4P_{12}$ but not in $LaFe_4P_{12}$. This supports theoretical assertions about the importance of f-orbital hybridization in the bonding of these compounds. Direct evidence for an occupied Ce 4f state in $CeFe_4P_{12}$ is seen in its valence band spectrum at a binding energy around 2.5 eV, similar to that in CeF_3. Comparison of the valence band spectra of $LaFe_4P_{12}$ and $CeFe_4P_{12}$ with theoretical density of states curves allows distinct energy regions of these spectra to be fit with component peaks that can be identified with parent atomic orbitals. The atomic charges derived from an electron population analysis of the intensities of these component peaks agree well with the formulations proposed above. This study provides a starting point for the more difficult analysis of other skutterudite-type compounds, particularly the antimonides, where electronegativity differences are considerably smaller than in the phosphides so valence state assignments will be even more challenging.

Acknowledgment. The Natural Sciences and Engineering Research Council (NSERC) of Canada supported this work through Discovery Grants to R.G.C. and A.M. Access to the Kratos XPS was kindly provided by the Alberta Centre for Surface Engineering and Science (ACSES) at the University of Alberta. ACSES is operated through capital funding from the Canada Foundation for Innovation (CFI), which also provides interim operating support, and Alberta Innovation and Science. A.P.G. thanks NSERC and the University of Alberta for support.

CM052623N

(45) Watts, J. F.; Wolstenholme, J. *An Introduction to Surface Analysis by XPS and AES*; Wiley: Rexdale, 2003.
(46) Brillson, L. J.; Ceasar, G. P. *Surf. Sci.* **1976**, *58*, 457−468.
(47) Scofield, J. H. *J. Electron Spectrosc. Relat. Phenom.* **1976**, *8*, 129−137.
(48) Tougaard, S. *QUASES-IMFP-TPP2M: Database for Calculation of IMFPs by TPP2M Formula*, version 2.1; QUASES-Tougaard, Inc.: Odense, Denmark, 2000 (www.quases.com).